

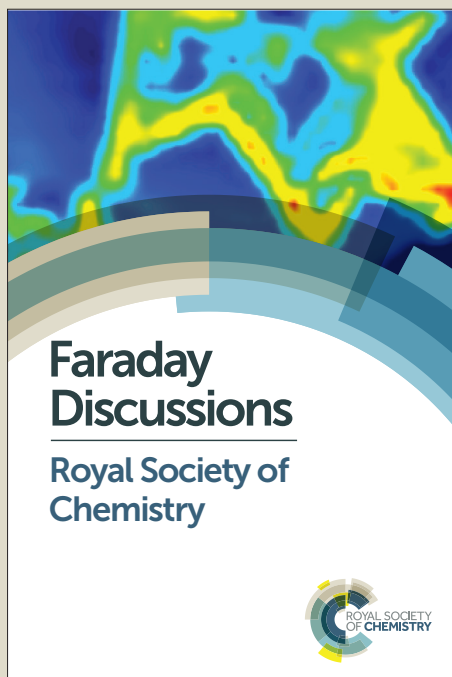
# Faraday Discussions

Accepted Manuscript



This manuscript will be presented and discussed at a forthcoming Faraday Discussion meeting. All delegates can contribute to the discussion which will be included in the final volume.

**Register now to attend!** Full details of all upcoming meetings: <http://rsc.li/fd-upcoming-meetings>



This is an *Accepted Manuscript*, which has been through the Royal Society of Chemistry peer review process and has been accepted for publication.

*Accepted Manuscripts* are published online shortly after acceptance, before technical editing, formatting and proof reading. Using this free service, authors can make their results available to the community, in citable form, before we publish the edited article. We will replace this *Accepted Manuscript* with the edited and formatted *Advance Article* as soon as it is available.

You can find more information about *Accepted Manuscripts* in the [Information for Authors](#).

Please note that technical editing may introduce minor changes to the text and/or graphics, which may alter content. The journal's standard [Terms & Conditions](#) and the [Ethical guidelines](#) still apply. In no event shall the Royal Society of Chemistry be held responsible for any errors or omissions in this *Accepted Manuscript* or any consequences arising from the use of any information it contains.

This article can be cited before page numbers have been issued, to do this please use: C. O'Brien, K. Dostert, M. Hollerer, C. Stiehler, F. Calaza, S. Schauer mann, S. Shaikhutdinov, M. Sterrer and H.-J. Freund, *Faraday Discuss.*, 2015, DOI: 10.1039/C5FD00143A.

## Supports and Modified Nano-particles in Designing Model Catalysts

C. P. O'Brien<sup>\*</sup>, K.-H. Dostert<sup>†</sup>, M. Hollerer<sup>‡</sup>, C. Stiehler<sup>†</sup>, F. Calaza<sup>†</sup>, S. Schauer<sup>†§</sup>, S. Shaikhutdinov<sup>†</sup>, M. Sterrer<sup>‡</sup>, H.-J. Freund<sup>†</sup>

Fritz-Haber Institut der Max-Planck Gesellschaft, Faradayweg 4-6, 14195 Berlin, Germany

### Abstract

In order to design catalytic materials, we need to understand the essential causes for material properties resulting from its composite nature. In this paper we discuss two, at first sight, diverse aspects:

- a) the effect of the oxide-metal interface on metal-nanoparticle properties and
- b) the consequences of metal particle modification after activation on the selectivity of hydrogenation reactions.

However, those two aspects are intimately linked. The metal-nanoparticles electronic structure changes at the interface as a catalyst is brought to different reaction temperatures due to morphological modifications in the metal and, as we will discuss, those changes the chemistry leading to changes in the reaction path. As the morphology of the particle varies, facets of different orientation and size are exposed which may lead to a change in surface chemistry as well.

We use two specific reactions to address those issues in some detail. To the best of our knowledge the present paper reports the first observations of this kind for well-defined model systems.

The changes of the electronic structure of Au nanoparticles due to their size and interaction with a supporting oxide are revealed as a function of temperature using CO<sub>2</sub> activation as a probe. The presence of spectator species (oxopropyl) as formed during an activation step of acrolein hydrogenation, strongly controls the selectivity of the reaction towards hydrogenation of the unsaturated C-O vs. the C-C bond on Pd(111) when compared with oxide supported Pd nanoparticles.

---

<sup>\*</sup> US Army Research Laboratory

<sup>†</sup> Fritz Haber Institute of the Max Planck Society, Department of Chemical Physics

<sup>‡</sup> Institute of Physics, University of Graz

<sup>§</sup> Institut für Physikalische Chemie, Christian-Albrechts-Universität zu Kiel

## Introduction

The properties of disperse metal catalysts are dominated by two factors: The size, morphology, and chemical modification of metal nanoparticles after having been activated, and the interaction of those nanoparticles, or small metal clusters, with the support, i.e. the metal-support interface. Those two factors are strongly interlinked and need to be addressed in model studies, if we want to understand their influence at the atomic level and find design principles for new catalytic material. This is described in this paper and exemplified by investigating two, seemingly different model systems.

There is no doubt that the metal-support interface is one of the determining factors in catalysis, as documented by many examples in the literature<sup>1</sup>, yet, it is not considered in most model studies. The electronic structure of the metal-support interface changes as the morphology of the metal particle may vary as a function temperature, for example, due to sintering. This may lead to the formation of particles with a variety of facets, which, in turn, changes the surface chemistry.<sup>2-5</sup>

Plausible explanations have been presented over the years for the “structure sensitivity” defined early on by Michel Boudart in connection with the function of the catalyst mainly refers to the size of a metal nanoparticle and relates to the various possible terminations with different facets.<sup>4-6</sup> This concept was taken as a basis for the surface science approach based on metal single crystal surfaces with respect to experiment,<sup>7,8</sup> and slab calculation in theory,<sup>9</sup> with varying terminations, the result of which could be used by superposition to explain the observed catalytic behavior. While in this approach, the support might be taken as the cause of the particular appearance of the nanoparticle, its chemical nature and specific interaction with the nanoparticle is not taken into account in such approaches.<sup>10</sup> The appearance of particles of different size and shape may cause a modification of the catalyst during the activation process. A series of attempts have been made in the literature, in order to consider material modification by the overgrowth of oxide films<sup>11</sup> or the incorporation of carbon in the surface<sup>2</sup> as well as subsurface areas which only then is turned into an effective hydrogenation catalyst.<sup>12</sup> Robert Schlögl<sup>13</sup> has recently presented a comprehensive review on the dynamic catalyst.

In the present paper we would like to address, both, the influence of the metal-oxide interface, as well as the influence of spectator species on selective hydrogenation, in an attempt

to exemplify design principles for new catalytic material. The present work is based on and a substantial extension of previous work on CO<sub>2</sub> activation on supported Au nanoparticles and on the competitive, selective hydrogenation of C-C vs. C-O double bonds on oxide supported Pd nanoparticles as a function of particle size. The paper is organized as follows: after a short description of the Experiments, we present and discuss the new results in comparison to the results obtained so far. We conclude with a summary and an outlook onto further experiments.

### Experimental Conditions

The experiments on supported Au nanoparticles on ultrathin MgO(100) films were carried out in different ultrahigh-vacuum (UHV) set-ups, all of them equipped with basic sample cleaning and preparation (sputtering, heating, evaporation, gas dosing) as well as characterization (low-energy electron diffraction, LEED) facilities. One of them had in addition a polarization modulation IRAS and a x-ray photoelectron spectroscopy (XPS) set-up attached. Infra-red spectra were acquired with a Bruker IFS66v FTIR spectrometer using a liquid-nitrogen cooled MCT detector. The XPS spectrometer is a SPECS type hemispherical analyzer (Phoibos 150) with a dual anode (Mg/Al) x-ray source. Scanning tunneling microscopy (STM) experiments have been carried out both at the Fritz Haber Institute using a home-built low-temperature STM operated at liquid helium temperature, as well as in the Physics Department of University of Graz using a CreaTec low-temperature STM operated at liquid-nitrogen temperature. The surface of the Ag(100) crystal used as a support for the MgO(100) films was cleaned by repeated sputter (Ar<sup>+</sup>, 800 V, 5 μA) - anneal (700 K) cycles and the cleanliness and surface quality was checked using LEED, as well as Auger spectroscopy and XPS. Preparation of the MgO films was carried out according to published recipes by reactive deposition of Mg in oxygen atmosphere ( $1 \times 10^{-6}$  mbar).<sup>14</sup> CO<sub>2</sub> was dosed from the background via a leak valve.

The experiments on acrolein hydrogenation on ironoxide supported Pd were performed with an ultra-high vacuum molecular beam machine that has been described in detail previously.<sup>15</sup> Molecular beams of acrolein and H<sub>2</sub> were directed at the sample simultaneously while the sample was held at constant temperature. The effusive molecular beams were produced by doubly differentially pumped multi-channel array sources. Acrolein (Sigma-Aldrich, 95% purity) was purified prior to each experiment by repeated freeze-pump-thaw

cycles. During all reactivity experiments the flux of H<sub>2</sub> on the sample surface was 4.8×10<sup>15</sup> molecules/cm<sup>2</sup>/s. The sample was exposed to H<sub>2</sub> for five minutes prior to acrolein exposure. The flux of acrolein on the sample surface was 1.5×10<sup>13</sup> molecules/cm<sup>2</sup>/s. Gas-phase fragments m/z = 56, 57, and 58 were detected with a quadrupole mass spectrometer (QMS) (ABB Extrel). Acrolein and the hydrogenation products propenol and propanal were identified by their fragmentation pattern in the QMS. Acrolein generates signals at m/z=56, 57, and 58 with intensity distribution of 1:0.04:0.01. Propenol causes signals at m/z=57 and 58 with intensity ratio of 1:0.1 and propanal was identified by signals at the same masses with the intensity distribution of 0.3:1. Surface species were detected simultaneously with gas-phase products using an infrared spectrometer (Bruker IFS 66v) with an MCT detector and a spectral resolution of 2 cm<sup>-1</sup>.

A well-ordered ~10 nm thick Fe<sub>3</sub>O<sub>4</sub> film was grown on a Pt(111) substrate (see <sup>16, 17</sup> for details) followed by Pd deposition onto the Fe<sub>3</sub>O<sub>4</sub> film at 120 K by physical vapor deposition of Pd (Goodfellow, >99.9%) using a commercial evaporator (Focus EFM 3). After depositing Pd, the sample was annealed at 600 K and the Pd nanoparticles were stabilized by repeated cycles of oxidation and reduction at 500 K.<sup>18</sup> The size of the Pd nanoparticles was controlled by the nominal thickness of the Pd film deposited onto the Fe<sub>3</sub>O<sub>4</sub> substrate at 120 K (see <sup>19</sup> for details) in comparison with STM images reported previously. The Pd(111) crystal was cleaned by repeated cycles of Ar<sup>+</sup> sputtering at room temperature, annealing at 1000 K, and oxidation in 1×10<sup>-6</sup> mbar O<sub>2</sub> at 750 K. The cleanliness of the Pd/Fe<sub>3</sub>O<sub>4</sub> and Pd(111) samples was verified prior to every experiment by infrared reflection absorption spectroscopy (IRAS) of adsorbed CO.

## Results and Discussion

### *Activation of Carbondioxide*<sup>20, 21</sup>

In a previous study<sup>21</sup> we had observed a scenario schematically represented by Figure 1. A two-layer MgO film was grown on an Ag(100) substrate, and Au was deposited from an Au evaporator at 77K, and annealed consecutively to 300K. It was noticed before that deposition at low temperature led to a two-dimensional growth of Au nanoparticles and islands<sup>22</sup>, as suggested by theoretical calculations.<sup>23</sup> The driving force for this unusual wetting of the oxide surface is an electron transfer from the Ag substrate through the film and collected by the Au islands, due to the large electron affinity of Au.<sup>23</sup> STM investigations, together with

model calculations had suggested that the charge in this metal-insulator-metal (MIM) system localizes at the rim of the nanoparticles, i.e. at the nanoparticle-oxide interface.<sup>24</sup> Having noticed this phenomenon a study of molecular adsorption was started. The first attempt was made using CO.<sup>25</sup> However, it turned out, that a direct imaging of the molecules was not possible, but inelastic spatially resolved electron tunneling spectra of the CO hindered translation at 45 meV provided evidence that those molecules do interact exclusively with the rim of the nanoparticle. It is interesting to note, that the CO molecules do not exhibit appreciable IR intensity.<sup>25</sup> This is indicative of a geometry leading to a small dipole moment perpendicular to the surface. Following up on this, we investigated the adsorption of a bigger molecule, isophorone, promising easier constant current imaging. It was possible to image the molecule at the rim, and, in addition, to study the consequences of adsorption onto the quantum well states of the nanoparticle, which develop due to its finite size.<sup>26</sup> In fact, the energetic position of quantum well states of one and the same nanoparticle was compared with those of the particle interacting with isophorone. Isophorone, as revealed by infrared spectroscopy, physisorbs on Au nanoparticles. This leads to a characteristic enhancement of the effective electron mass of the Au electrons, in line with physisorption. While this is important to understand the details of the molecule-nanoparticle interaction, those observations do not provide evidence for a reaction. This came from studies of CO<sub>2</sub> adsorption on those systems.<sup>21</sup> When CO<sub>2</sub> adsorbs on the surface it locates at the rim of the clusters and transforms to CO<sub>2</sub><sup>-</sup> (see Figure 1) by electron transfer from the Au nanoparticle. While this process is energetically uphill by 0.6 eV, the presence of additional CO<sub>2</sub>, able to “solvate” the carboxylate to a (CO<sub>2</sub>)<sub>2</sub><sup>-</sup> dimer ion, leads to a 1.6 eV downhill process. Spectroscopic studies, further elaborated and extended on below suggest together with model calculations that this finally results in an oxalate ion, by a second electron transfer, all happening at the rim of the nanoparticle.

Figure 2 shows a set of infrared spectra of the surface as a function of annealing temperature. First we concentrate on the trace recorded at lowest temperature. The peak at 1295 cm<sup>-1</sup> is due to CO<sub>2</sub> adsorption on the oxide support forming a carboxylate, i.e. not a carbonate (!) at specific sites of the MgO film. The two bands at 1220 cm<sup>-1</sup> and 1440 cm<sup>-1</sup> have been identified as being due to the oxalate species. This spectrum is entirely consistent with the spectra recorded before.<sup>21</sup> The other spectra in Figure 2 have been taken after annealing the Au deposits at higher temperature. Obviously, annealing at higher temperature does not

influence intensities in the infrared spectra massively, unless the system is annealed at or higher than 500K. This is also consistent with our previous findings using temperature programmed desorption, where oxalate dissociation into two CO<sub>2</sub> molecules started to occur well below this temperature. If one annealed not quite to this temperature the process of oxalate formation was entirely reversible. This hinted towards a kinetically controlled process that changes the system.

Ricci et al,<sup>23</sup> in a landmark paper, had demonstrated, that for nanoparticles on ultrathin oxide films, the electron transfer through the film depends strongly on the dimensionality of the Au particle on the oxide. Clearly, a two-dimensional particle was prone to accept more electronic charge than a three-dimensional particle, and it also depended considerably on the contact area of the particle. Given this scenario, one might envision, that by increasing the mobility of the Au atoms on the oxide film through annealing at higher temperature, three-dimensional particles start to grow on the film. Those particles would exhibit small enough charge transfer that the chemical potential for forming the CO<sub>2</sub> anion and the oxalate is impossible. This would establish the first proof of a morphology driven change in reaction at the oxide metal interface. In order to see whether this would be a valid interpretation, we performed and present here an STM study that is summarized in Figure 3. It shows a set of STM images taken at different annealing temperatures. Figure 3a has been recorded at 77 K and reveals Au adsorbed as single atoms or small clusters. Annealing to room temperature or slightly above (Figure 3b) causes two-dimensional islands to form all over the surface. Their average size varies between 3 and 5 nm with variability in shape ranging from roundish (hexagonal) islands to more rectangular (raft like) ones. This is consistent with our previous findings.<sup>22</sup> Increasing the temperature to 400 K increases the average islands diameter to 4-8 nm but does not change the growth mode (Figure 3c). The drastic change occurs if the annealing temperature is raised to 500K (Figure 3d). We find a cross over to three-dimensional growth with particle diameters between 5 and 10nm and 1-2 nm height. There are still a few two-dimensional islands observed, but most of the Au is contained in 3D particles.

Using this information we may now return to a discussion of Figure 2, and try to understand the changes of the oxalate signals as a function of temperature. As stated above, the lowest trace represents the oxalate species at the rim of the 2D nanoparticles, as proven in previous



reports.<sup>21</sup> The infrared spectra start to attenuate and significantly change after the system has been either prepared at temperatures higher than app. 500 K, or annealed sufficiently long at that temperature. We know from the above STM study, that this is concomitant with the change from 2D to 3D morphology. As referred to above, as well, the formation of the 3D particles reduces the electron transfer from the Ag substrate, and, we conclude, must be the reason for the reduced ability to form oxalate species. Note, that the species due to adsorption on the MgO film at  $1295\text{ cm}^{-1}$  is not influenced by the change in growth mode.

At the present time, theoretical modeling of the process, which would be highly desirable, is not possible. Hannu Häkkinen and his group have greatly contributed to our understanding of the oxalate formation as documented in ref.<sup>21</sup>. However, a full, detailed description involving nanoparticles of the size observed experimentally seems to be out of range at present. Schematically, as depicted in Figure 1, this means a change from reacting  $\text{CO}_2$  at nanoparticles (2D) towards unreactive particles in 3D morphology. To the best of our knowledge this is the first clear experimental indication for such a behavior.<sup>27</sup>

In order to relate the finding reported in this paper to the design of real powder based catalysts we refer to our study showing that doping of bulk oxides with transition metals<sup>28</sup>, which provide the electron source to trigger a similar control of morphology as the Ag support of the ultrathin film. It will be the task of future work to experimentally establish this in model systems and in powder samples. However, based on the findings reported here, one may envision to control and design  $\text{CO}_2$  activation catalysts by doping induced charge transfer, and thus establish a design principle for supported Au catalysts.

#### *Hydrogenation of Acrolein*<sup>29</sup>

Hydrogenation of C-C double bonds has been shown to depend on the presence of hydrogen atoms absorbed inside the metal nanoparticles.<sup>2</sup> The absorbed hydrogen provides the pool to sustain catalytic activity. Carbon and/or carbonaceous deposits adsorbed at the particles corners and edges control the diffusion of the hydrogen necessary for hydrogenation from below the surface to the surface of the particle. The selective, competitive hydrogenation of acrolein, i.e. the hydrogenation of a C-C double bond versus the hydrogenation of a C-O double bond, represents an even more ambitious situation.<sup>29</sup>



In a previous study,<sup>29</sup> we investigated the selectivity of the partial hydrogenation of acrolein on a Pd(111) single crystal and on Pd/Fe<sub>3</sub>O<sub>4</sub> model catalysts by isothermal molecular beam experiments under well-defined UHV conditions. The formation of gas-phase products was detected by quadrupole mass spectrometry (QMS); simultaneously, the evolution of surface species was investigated by infrared reflection-absorption spectroscopy (IRAS) studies. Pd(111) and Pd/Fe<sub>3</sub>O<sub>4</sub> showed very different selectivity in partial hydrogenation of acrolein. Over Pd/Fe<sub>3</sub>O<sub>4</sub>, selective conversion of acrolein to propanal occurs, while over a Pd(111) single crystal, propenol is formed with near 100% selectivity. IRAS studies on the surface turning over showed that the selectivity to propenol formation on Pd(111) critically depends on the presence of a dense overlayer of an oxopropyl species formed at an initial stage of acrolein and hydrogen exposure. On the modified Pd(111) surface, acrolein is adsorbed via the C=O bond and reacts to propenol. On Pd/Fe<sub>3</sub>O<sub>4</sub>, however, significantly different surface chemistry occurs under identical experimental conditions. Instead of forming an oxopropyl layer, a fraction of the acrolein molecules decomposes forming CO molecules and C<sub>x</sub>H<sub>y</sub> fragments that eventually block all Pd sites while the propanal formation rate decreases to zero. Most likely, low-coordinated surface sites and (100) facets of the Pd clusters are responsible for the rapid acrolein decarbonylation. The reason for the significantly different surface chemistry on Pd/Fe<sub>3</sub>O<sub>4</sub> and Pd(111), however, needs further investigation. In particular, a detailed kinetic analysis of all possible reaction pathways on the different Pd surfaces would be required. Nevertheless, our investigations unambiguously show that the modification of the Pd(111) surface with a dense oxopropyl overlayer correlates with a change in selectivity from propanal to propenol formation. Moreover, the absence of the oxopropyl layer on Pd/Fe<sub>3</sub>O<sub>4</sub> seems to be related to the decarbonylation of acrolein.

Based on our previous results, we have addressed the question whether it is possible to also produce propenol on Pd/Fe<sub>3</sub>O<sub>4</sub> model catalysts. We could think about a large number of different approaches, such as modifying the Pd clusters prior to acrolein conversion, *e.g.* by pre-adsorbed CO or hydrocarbons or by C modification of low-coordinated Pd sites. In the present study, however, we focus on the effect of Pd particle size. We have investigated the hydrogenation of acrolein on 7 nm and 12 nm Pd particles using molecular beam techniques under isothermal conditions. The formation of the gas-phase products has been detected by QMS and the surface composition has been simultaneously investigated by IRAS. In all exper-

iments, the surface has been pre-exposed to  $4.8 \cdot 10^{15}$  H<sub>2</sub>/(cm<sup>2</sup>·s) for 300 s before the acrolein beam with  $1.5 \cdot 10^{13}$  molecules/(cm<sup>2</sup>·s) has additionally been switched on.

Figure 4 shows the formation rates of the partial hydrogenation products on Fe<sub>3</sub>O<sub>4</sub>-supported 7 nm and 12 nm Pd particles detected in the gas phase. With both particles sizes, similar propanal formation rates are observed, which pass through a maximum after about 30 s and then decrease to zero. On 12 nm particles, however, additionally a small amount of propenol is detected. The propenol production rate rapidly increases after about 40 s, when the propanal formation has almost stopped, passes a maximum after about 60 s and finally decreases to zero. In general, both partial hydrogenation products have been identified by their characteristic fragmentation pattern in QMS. The clearly different time dependence of the two product formation rates in this study, however, provides an additional possibility to unambiguously distinguish between propanal and propenol. Nevertheless, the total amount of propenol that is formed on the 12 nm particles is much smaller than on a Pd(111) single crystal. It should be noted that formation of gas-phase propenol has only been detected in a narrow temperature range near 250 K. It was not observed in our previous studies on Pd particles under slightly different conditions such as a lower or higher surface temperature or when using a pulsed acrolein beam instead of continuous exposure.

Figure 5 illustrates the correlation between the evolution of propenol in the gas phase detected by QMS and the formation of surface species on the 12 nm Pd particles turning over studied by IRAS. A time-dependent series of IR spectra obtained with a time resolution of 45 s is shown in Figure 5a. IR absorption features appear near 1855 cm<sup>-1</sup>, 1755 cm<sup>-1</sup>, and 1670 cm<sup>-1</sup>. The vibration at 1670 cm<sup>-1</sup> is most likely associated with the C=O stretching in molecularly adsorbed acrolein. It has been assigned to acrolein adsorbed on a Pd(111) single crystal in a previous study.<sup>29</sup> The adsorbate giving rise to the IR absorption near 1755 cm<sup>-1</sup> accumulates at the beginning of the acrolein exposure and saturates during the first 45 s. Interestingly, this band has previously been related to the oxopropyl species modifying the Pd(111) surface for propenol production. The IR vibration at 1855 cm<sup>-1</sup> most likely shows CO adsorbed on the Pd(111) facets. The slowly increasing IR absorption intensity indicates a rather slow accumulation of CO, most likely from acrolein decarbonylation. Hence, the decarbonylation of acrolein is significantly less efficient at 250 K as compared to our previous studies at 270 K. Figure 5b illustrates the simultaneously recorded propenol evolution in the

gas phase. A clear onset is observed after about 40 s, which is approximately when the oxopropyl species saturates.

The simultaneously performed IRAS and QMS studies on the 12 nm Pd particles turning over at 250 K give detailed insights into the mechanism of the acrolein conversion. On the one hand, our results strongly reveal that also on the 12 nm particles a modification of the surface by an oxopropyl layer triggers the propenol production. In contrast to Pd(111), however, the additional presence of acrolein and CO on the surface reveals that the oxopropyl species is not covering the whole Pd surface with a dense layer. On the other hand, it is again indicated that the decarbonylation of acrolein has to be avoided to form propenol on Pd particles. By reducing the surface temperature from 270 K to 250 K the decarbonylation of acrolein is largely suppressed while the temperature is still high enough to form a small amount of propenol. It seems that the temperature needs to be carefully chosen to keep the decarbonylation reaction rate as low as possible while the propenol formation rate should still be sufficiently high.

Our studies show a significant particle size dependence of the selectivity in partial hydrogenation of acrolein over Pd model catalysts at 250 K. On both 7 nm and 12 nm Pd particles, a similar amount of propanal is formed. Hydrogenation of acrolein to propenol, in contrast, appears possible only on 12 nm particles. The clearly different time dependence of propanal and propenol evolution agrees well with our previous findings showing propanal formation as long as pristine Pd is available and propenol production, in contrast, after a dense oxopropyl overlayer is formed. It seems that the selectivity towards propenol formation increases with increasing Pd cluster size from 0% on 7 nm Pd particles and a small amount over 12 nm Pd particles to approximately 100% on a Pd(111) single crystal. Possibly, the formation of an oxopropyl layer in sufficiently large domains is necessary to produce propenol, which is more likely to happen on larger Pd clusters having larger (111) facets and a lower concentration of low-coordinated sites. Low-coordinated sites, such as edges, corners, and defects may catalyze the acrolein decarbonylation.

### Synopsis

The present study clearly points to two important factors influencing catalytic activity of supported metal nanoparticles, which influence the design of new catalytic material:

- The interaction with the support controls the size and shape of the nanoparticle, and, in particular, the charge exchange and transfer at the oxide-metal interface. Specifically designed model systems allow us to isolate details of the problem and study them at the atomic level. Here, the surface science approach turns out to be the method of choice to image and characterize molecules interacting with the metal particle at the metal-oxide interface using a combination of scanning probe and spectroscopic techniques. This has allowed, for the first time, to directly identify the consequence of molecular adsorption and reaction on the electronic structure of a metal nanoparticle. Temperature is decisive in determining the mobility of metal atoms and particles on supports. We show in this paper, that a change in particle morphology controls the reactivity of the system at the oxide-metal interface, as the transition from two-dimensional Au particles at lower temperature to three-dimensional growth at higher temperature reduces the charge transfer from the support to the metal nanoparticle.
- Adsorbed species formed during a reaction which are not turned over, have been identified to modify a supported metal nanoparticle, and via this modification control the selectivity of a hydrogenation reaction. The selective hydrogenation of acrolein has been studied as an example. In particular, an oxopropyl species formed from adsorbed acrolein modifies the surface in such a way that acrolein hydrogenation leads to propenol and the hydrogenation of the C-C double bond is avoided. We had demonstrated before that Pd(111) single crystals selectively hydrogenate the C-O bond in acrolein, while supported Pd nanoparticles exclusively hydrogenate the C-C bond. We show in this paper, that there is a particle size effect. The particle needs to have a certain size in order to expose (111) facets of sufficient size to favor the effect. If particles are smaller, presumably the presence of edges, corners and irregularities in the particles favor the formation of CO, which poisons the oxopropyl effect.

The knowledge derived from both those observations can be used to design catalytic material and to control catalytic reaction.

## Acknowledgement

We are grateful to the German Science Foundation through the cluster of Excellence Unicast (administered by the TU Berlin) as well as the Fonds der Chemischen Industrie or financial support. F. Calaza thanks the Alexander von Humboldt foundation for a Georg Forster Research Fellowship. C. Stiehler thanks the Studienstiftung des Deutschen Volkes for a fellowship. S. Schauerermann is grateful to the European Research Council for a Starting Grant "Enantioselective Reactions on Model Chirally Modified Surfaces". M. Sterrer acknowledges support by the European Research Council through Grant Agreement No. 280070 (STRUBOLI).

## References:

1. H. K. G. Ertl, F. Schüth and J. Weitkamp, *Handbook of Heterogeneous Catalysis*, VCH, Wiley-VCH, Weinheim, compl. rev. and enlarged ed. edn., 2008.
2. M. Wilde, K. Fukutani, W. Ludwig, B. Brandt, J.-H. Fischer, S. Schauerermann and H. J. Freund, *Angew. Chem. Int. Ed.*, 2008, **47**, 9289-9293.
3. S. J. Thomson and G. Webb, *J. Chem. Soc., Chem. Commun.*, 1976, **13**, 526-527.
4. G. C. Bond, *Metal-Catalysed Reactions of Hydrocarbons*, Springer US, New York, 2005.
5. J. Sauer and H.-J. Freund, *Catal. Lett.*, 2015, **145**, 109-125.
6. M. Boudart and G. Djega-Mariadassou, *Journal*, 1984.
7. G. Ertl, *Angew. Chem. Int. Ed.*, 2008, **47**, 3524-3535.
8. G. Ertl and H. J. Freund, *Phys Today*, 1999, **52**, 32-38.
9. J. Sauer, *Chem. Rev.*, 1989, **89**, 199-255.
10. H. J. Freund, N. Nilius, T. Risse and S. Schauerermann, *Phys. Chem. Chem. Phys.*, 2014, **16**, 8148-8167.
11. S. Shaikhutdinov and H.-J. Freund, *Annu. Rev. Phys. Chem.*, 2012, **63**, 619-633.
12. D. Teschner, J. Borsodi, A. Wootsch, Z. Révay, M. Hävecker, A. Knop-Gericke, S. D. Jackson and R. Schlögl, *Science*, 2008, **320**, 86-89.
13. R. Schlögl, *Angew. Chem. Int. Ed.*, 2015, **54**, 3465-3520.
14. J. Pal, M. Smerieri, E. Celasco, L. Savio, L. Vattuone and M. Rocca, *Phys. Rev. Lett.*, 2014, **112**, 126102.
15. J. Libuda, I. Meusel, J. Hartmann and H.-J. Freund, *Rev. Sci. Instrum.*, 2000, **71**, 4395.
16. W. Weiss and W. Ranke, *Progr. Surf. Sci.*, 2002, **70**, 1-151.
17. C. Lemire, R. Meyer, V. E. Henrich, S. Shaikhutdinov and H. J. Freund, *Surf. Sci.*, 2004, **572**, 103.
18. T. Schalow, B. Brandt, D. Starr, M. Laurin, S. Schauerermann, S. Shaikhutdinov, J. Libuda and H. J. Freund, *Catal. Lett.*, 2006, **107**, 189-196.
19. T. Schalow, B. Brandt, D. E. Starr, M. Laurin, S. K. Shaikhutdinov, S. Schauerermann, J. Libuda and H. J. Freund, *Phys. Chem. Chem. Phys.*, 2007, **9**, 1347-1361.
20. H.-J. Freund and M. W. Roberts, *Surf. Sci. Rep.*, 1996, **25**, 225-273.

21. F. Calaza, C. Stiehler, Y. Fujimori, M. Sterrer, S. Beeg, M. Ruiz-Oses, N. Nilius, M. Heyde, T. Parviainen, K. Honkala, H. Häkkinen and H.-J. Freund, *Angew. Chem. Int. Ed.*, 2015, **54**, 12484.
22. M. Sterrer, T. Risse, U. Martinez Pozzoni, L. Giordano, M. Heyde, H.-P. Rust, G. Pacchioni and H.-J. Freund, *Phys. Rev. Lett.*, 2007, **98**, 096107.
23. D. Ricci, A. Bongiorno, G. Pacchioni and U. Landman, *Phys. Rev. Lett.*, 2006, **97**, 036106.
24. X. Lin, N. Nilius, M. Sterrer, P. Koskinen, H. Haekkinen and H.-J. Freund, *Phys. Rev. B*, 2010, **81**, 153406.
25. X. Lin, B. Yang, H. M. Benia, P. Myrach, M. Yulikov, A. Aumer, M. Brown, M. Sterrer, O. Bondarchuk, E. Kieseritzky, J. Rucker, T. Risse, H. Gao, N. Nilius and H. J. Freund, *J. Am. Chem. Soc.*, 2010, **132**, 7745-7749.
26. C. Stiehler, F. Calaza, W.-D. Schneider, N. Nilius and H.-J. Freund, *Phys. Rev. Lett.*, 2015, **115**, 036804.
27. M. Chen and D. W. Goodman, *Chem. Soc. Rev.*, 2008, **37**, 1860-1870.
28. X. Shao, S. Prada, L. Giordano, G. Pacchioni, N. Nilius and H.-J. Freund, *Angew. Chem. Int. Ed.*, 2011, **50**, 11525-11527.
29. K.-H. Dostert, C. P. O'Brien, F. Ivars-Barcelo, S. Schauer mann and H.-J. Freund, *J. Am. Chem. Soc.*, 2015, **submitted**.

## Figures

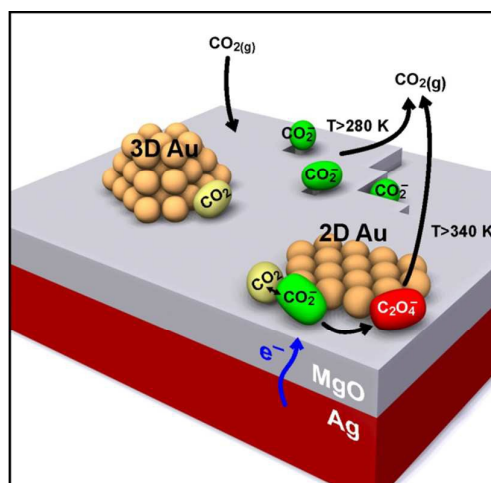


**Figure 1:** Schematic showing the individual steps of oxalate formation upon chemisorption of  $\text{CO}_2$  on the rim of 2D Au islands on thin MgO(001)/Ag(001) films.<sup>21</sup> Carboxylate species (green) are formed both on defect sites of the MgO film and on the rim of the 2D Au islands by electron transfer. Only on the latter, additional  $\text{CO}_2$  (yellow) is able to solvate the carboxylate species yielding a  $(\text{CO}_2)_2^-$  dimer ion, which, after an additional electron transfer, results in adsorbed oxalate  $\text{C}_2\text{O}_4^{2-}$  (red). This reaction does not occur on 3D Au particles.

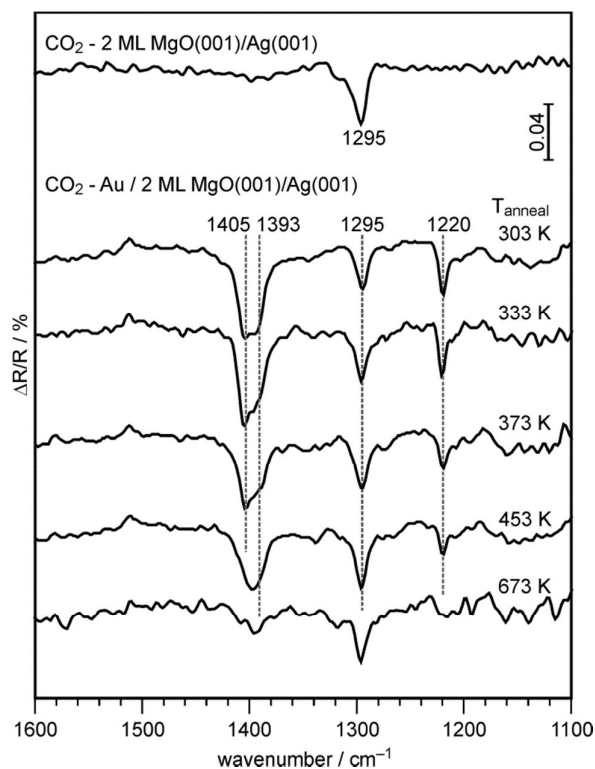


**Figure 2:** IRA spectra of bare (top) and Au-loaded 2 ML MgO(001)/Ag(001) samples recorded after a saturation dose of  $\text{CO}_2$  at 223 K. Au was deposited at 100 K and the samples subsequently annealed to the indicated temperature prior to  $\text{CO}_2$  adsorption.



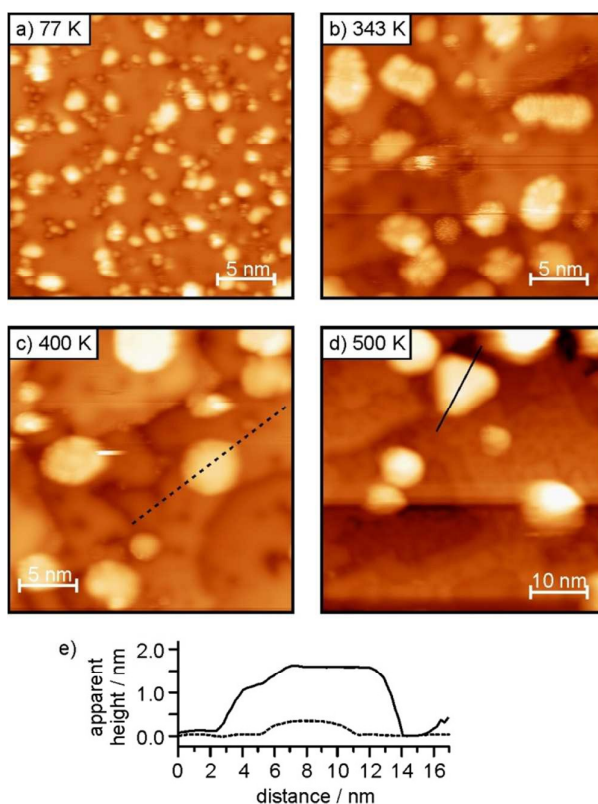


**Figure 3:** STM images of (a) Au deposited on 2 ML MgO(001)/Ag(001) at 77 K, and after subsequent annealing of the system to 343 K (b), 400 K (c) and 500 K (d). All images were taken at 77 K. Scan area: (a)-(c) 25 nm × 25 nm; (d) 50 nm × 50 nm.  $U_{\text{bias}} = +(0.5\text{--}0.75)$  V.  $I_t = 30$  pA. e) Height profiles of representative islands/particles from the 400 K (dashed line) and 500 K (dotted line) annealed samples, highlighting the transition from 2D to 3D geometries.

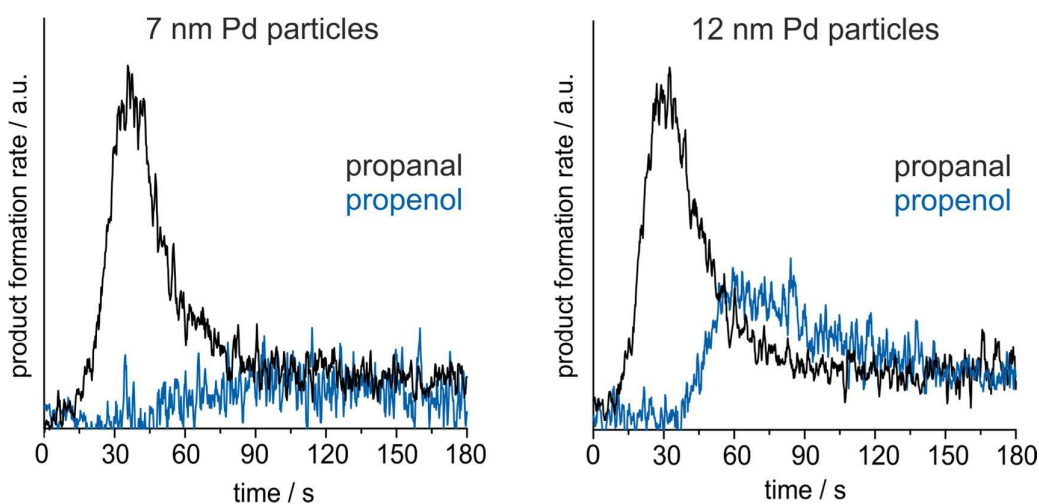


**Figure 4:** Formation rates of propanal (black lines) and propenol (blue lines) over  $\text{Fe}_3\text{O}_4$ -supported Pd particles with diameters of 7 nm (left) and 12 nm (right) at 250 K detected by QMS.

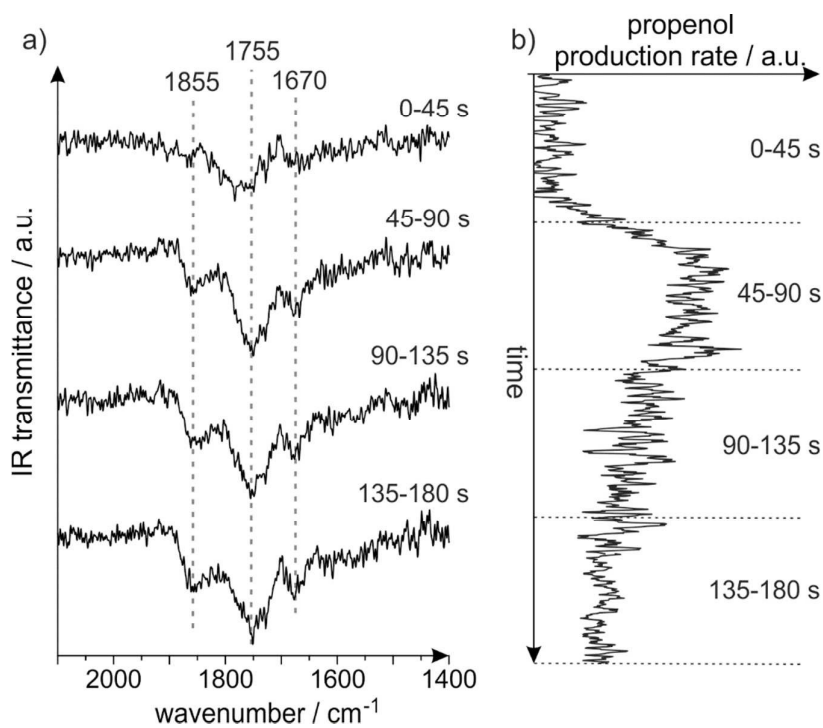


**Figure 5:** (a) Time-resolved IR spectra monitor the evolution of surface species on 12 nm Pd particles turning over and (b) QMS measurements show the formation rate of propenol in the gas phase simultaneously.